Downloaded from orbit.dtu.dk on: May 05, 2023

DTU Library

Synthetic Aperture Focusing for a Single Element Transducer undergoing Helix Motion

Andresen, Henrik; Nikolov, Svetoslav Ivanov; Jensen, Jørgen Arendt

Published in:
I E E E Transactions on Ultrasonics, Ferroelectrics and Frequency Control

Link to article, DOI:
10.1109/TUFFC.2011.1894

Publication date:
2011

Document Version
Early version, also known as pre-print

Link back to DTU Orbit

Citation (APA):
Andresen, H., Nikolov, S. I., & Jensen, J. A. (2011). Synthetic Aperture Focusing for a Single Element Transducer undergoing Helix Motion. *I E E E Transactions on Ultrasonics, Ferroelectrics and Frequency Control*, *58*(5), 935-943. https://doi.org/10.1109/TUFFC.2011.1894

General rights
Copyright and moral rights for the publications made accessible in the public portal are retained by the authors and/or other copyright owners and it is a condition of accessing publications that users recognise and abide by the legal requirements associated with these rights.

- Users may download and print one copy of any publication from the public portal for the purpose of private study or research.
- You may not further distribute the material or use it for any profit-making activity or commercial gain
- You may freely distribute the URL identifying the publication in the public portal

If you believe that this document breaches copyright please contact us providing details, and we will remove access to the work immediately and investigate your claim.

Synthetic Aperture Focusing for a Single Element Transducer undergoing Helix Motion

Henrik Andresen[1,2], Svetoslav Ivanov Nikolov[2] and Jørgen Arendt Jensen[1]

1) Center for Fast Ultrasound Imaging, DTU Elektro,
Bldg. 348, Technical University of Denmark, DK-2800 Lyngby, Denmark.
2) B-K Medical, Mileparken 34, DK-2730 Herlev, Denmark.

***Abstract*—This paper describes the application of 3D synthetic aperture focusing (SAF) to a single element trans-rectal ultrasound transducer. The transducer samples a 3D volume by simultaneous rotation and translation giving a helix motion. Two different 3D SAF methods are investigated, a direct and a two-step approach. Both methods perform almost identical for simulated scatterers and give a significant improvement in azimuth resolution and a constant resolution in elevation. Side-lobes below -60 dB is achievable for both methods.**

Validation of the method is achieved by scanning a simple wire phantom and a complex phantom containing wires in azimuth and elevation. The simple wire phantom shows the same results as that found through simulation. The complex phantom shows simultaneous focusing in azimuth and elevation for the wire scatterers.

Considerations on processing requirements for both 3D SAF methods show that the two-step approach can give equivalent performance using an order of magnitude lower calculations. This reduction requires a temporary storage of 9.1 GB of data for the investigated setup.

I. Introduction

Males living in the United States have a risk of 16.7% for developing prostate cancer during their lifetime, which accounts for 25% of all cancer cases in males [1]. Some of the prostate cancer cases are treated by radioactive seed implantation, also called brachytherapy. The treatment depends on a pre-operation analysis of the prostate to decide on seed placements, which can be done using either x-ray computed tomography (CT) or trans-rectal ultrasound (TRUS). During the procedure the prostate will move and change dimensions due to a different patient position and needle insertion. For a better placement of the seeds a real-time visualization of the prostate gland is desired. X-ray CT is of limited use due to both radiation exposure of medical staff as well as limitations of the machines. Using 3D TRUS to visualize the prostate gland during operation allows for an interactive guided placement of the seeds [2].

TRUS transducers are made of both single-element and array transducers. Single-element transducers are cheaper to produce and have lower requirements on sampling and connectivity compared to multi-element transducers. It is possible to acquire 3D volume data by applying rotation and translation simultaneously. The transducer design investigated in this paper is a single-element TRUS probe primarily designed to investigate the rectal wall. The results gained here can easily be translated to rotating transducer arrays, especially if combined by a sequential beamforming as presented in [3].

Single element transducers have a good image quality for a limited region of depth. Outside this region the resolution quickly degrades both in azimuth and elevation. This can be alleviated by synthetic aperture focusing (SAF). SAF is a method originally used in radar systems [4]. This method was later applied to ultrasound imaging for medical use [5]–[7]. SAF has been shown to be able to increase the resolution and signal-to-noise ratio outside this region by focusing the received signal from several emissions for either translating or rotating movements [8]–[10]. By increasing the focal region, it is possible to extend the range of use for a given transducer. Measurements will also be less susceptible to differences in patient size and anatomy.

This paper investigates the effects of performing 3D SAF with a single element transducer undergoing a helix motion. The paper shows the effects on the full width at half max (FWHM), mean side-lobe level (MSLL), and signal-to-noise ratio (SNR) for single plane focusing, as well as 3D focusing using a two-step focusing or direct 3D focusing for each emission. Initial analysis is made using simulations with Field II [11], [12]. Validation of the simulations is done using two wire phantoms.

Section II describes the method being used to perform SAF, Section III describes the equipment used and parameters for simulations and Section IV shows the results obtained. Since full 3D focusing requires much more processing than simply doing scan-conversion, the requirements on processing is discussed in Section V.

II. Method

Conventional imaging using a single element fixed focus transducer shows the amplitude detected signal for each emission using a scan-conversion appropriate for the transducer motion. Outside the focal depth of the transducer, the response will contain information from tissue outside the center-line of the element, degrading the resolution of the image. Monostatic synthetic aperture focusing (SAF) can combine several emissions for each image line. By applying different delays to each emission it is possible to achieve dynamic focusing outside the focal-point of a fixed focus transducer. This focusing is achieved because of the transducer motion, creating a

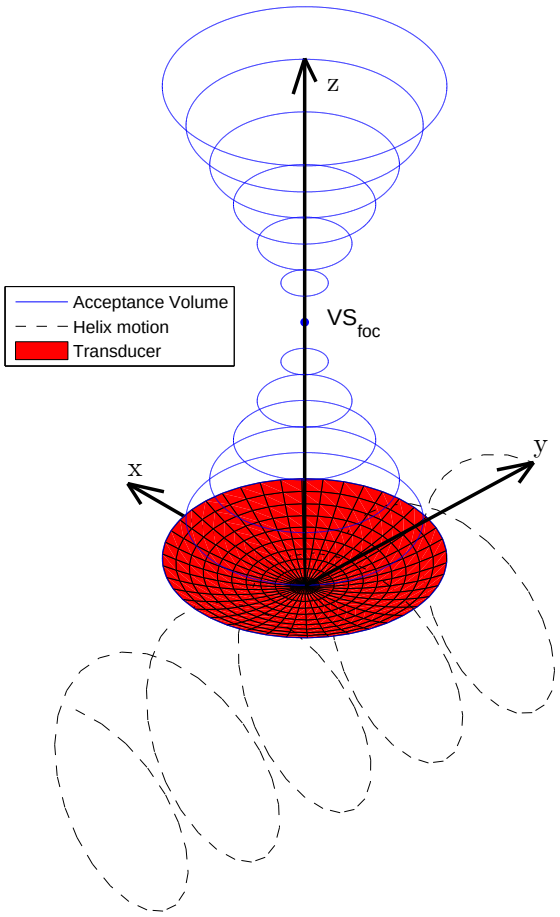

Figure 1. Visualization of the motion and virtual source for the transducer. The blue rings show the limits of the acceptance volume, the black dotted line shows the motion of the element and the large surface represents the actual transducer.

synthetic aperture.

Conventional SAF assumes a defocused spherical wave is emitted from the transmitting element, propagating in all directions. Single element transducers are often mechanically focused and will not emit a defocused spherical wave. Instead, the focal point of the transducer can be viewed as a virtual source (VS), emitting a spherical wave within a limited angle of divergence along the central direction of propagation [13]–[16]. Fig. 1 shows the setup as used in this paper. The transducer is shown as a concave surface with a focal point denoted by $\mathrm{VS}_{\mathrm{foc}}$. The transducer will move along the dotted line and rotate so the z-axis will point from the center of the cylinder to the outside, making it perpendicular to the line. The rings along the z-axis show the limits of the acceptance angle, which are rotationally symmetric, defining a volume of acceptance. Within the acceptance angle, the assumption of a spherical wave propagation is assumed to be valid.

The time-of-flight (ToF) for a given point of interest within the volume of acceptance is given by

$$T(\vec{r}_p) = \frac{2}{c}\left(|\vec{r}_p - \vec{\mathrm{VS}}_{\mathrm{foc}}| \cdot \frac{r_{p,z} - z_{VS}}{|r_{p,z} - z_{VS}|} + z_{VS}\right), \quad (1)$$

where c is the speed of sound, $\vec{r_p}$ is the point of interest, $\vec{\mathrm{VS}}_{\mathrm{foc}}$ is the position of the virtual source, $r_{p,z}$ is the depth of the point of interest, and z_{VS} is the depth of the virtual source. It is assumed that the transducer is positioned at $\vec{r} = (0, 0, 0)$ and the direction of propagation is along the z-axis for easier notation. The acceptance angle can be expressed as

$$\theta = \tan^{-1}\left(\frac{h}{2z_{\mathrm{VS}}}\right), \quad (2)$$

where h is the height of the transducer. Widening the acceptance angle allows more emissions to be combined for a single point. A downside of this change will be that the resolution will degrade more quickly outside the focal region, if used for conventional imaging.

The resolution attainable from SAF is dependent on the $F^{\#}$ that it is possible to synthesize. If the transducer is only translating, it is possible to calculate the maximum valid aperture, denoted L, depending on the depth relative to the virtual source from (2). We can now calculate

$$\begin{aligned} F^{\#}_{\mathrm{SAF}} &= \frac{L}{|z - z_{\mathrm{VS}}|} \\ F^{\#}_{\mathrm{SAF}} &= \frac{2\tan(\theta)|z - z_{\mathrm{VS}}|}{|z - z_{\mathrm{VS}}|} \\ F^{\#}_{\mathrm{SAF}} &= \frac{h}{z_{\mathrm{VS}}} = F^{\#}_{\mathrm{xdc}} \end{aligned} \quad (3)$$

where $F^{\#}_{\mathrm{SAF}}$ is the best possible synthesized f-number and $F^{\#}_{\mathrm{xdc}}$ is the f-number of the transducer. This shows that for pure translation SAF is able to maintain the same resolution for all depths, which the transducer has at the focal point. Since the transducer is rotating in the other direction, the expression becomes more complex and the result can be approximated as a linear increase as a function of depth [17].

The beamformed signal for a single point is calculated by

$$p(\vec{r}) = \sum_{n=1}^{N} a_n s_n(T_n(\vec{r})), \quad (4)$$

where N is the total number of contributing emissions, a_n is the apodization for the n'th emission, $s_n(t)$ is the received signal from the n'th emission at time t, and $T_n(\vec{r})$ is the ToF. As the transducer is both moving and rotating, the coordinate system is rotated around the transducer to allow the ToF calculations to be made by (1).

A. 3D beamforming schemes

For 3D SAF beamforming two approaches are investigated in this paper. The first is doing the ToF calculations for a given point directly from all contributing emissions according to (4). This generates a large number of calculations, but has a single ToF value for each sample and only relies on a single interpolation to acquire the RF sample. Another approach is described in [18]. This two-step method applies 2D beamforming first in azimuth by improving resolution in each scan-plane separately, which compares to using conventional 2D

SAF. Although the transducer moves in a helix, the translation per rotation is small enough to allow the translatory effect to be neglected. The lines in the scan-planes are then used as data for a subsequent focusing in the elevation direction. A benefit from this method is firstly, a large reduction in the number of required calculations and secondly, that any method can be used to generate the initial azimuth focused data. Drawbacks are the method requires two interpolations and creates a potentially large temporary dataset. The axial sampling density for the first beamforming step is estimated from [19] and given by

$$N = \frac{4d(1 + \frac{B_{\text{rel}}}{2})}{\lambda}, \tag{5}$$

where d is the sampling depth, B_{rel} is the relative bandwidth of the transducer, and λ is the wave-length of the center frequency of the emitted pulse. The angular sampling density is equal to the number of lines per revolution.

Both ToF schemes can be calculated using the method described in [20], which has the same computational requirement per point regardless of whether 2 or 3 dimensions are used. This makes comparison in computational costs simpler since only the actual number of points will be significant.

III. Measurement Setup

All measurements are performed using a scanner system supplied by BK-Medical, Herlev, Denmark. The transducer element undergoes a helix motion with 900 emissions per revolution and a movement of 0.2 mm in elevation per revolution. The transducer parameters are found in Table I. The scanner supplies complex RF-data sampled at 12 MHz at baseband. Data are moved from the scanner to a capture PC in real-time with a Camera Link interface card from Dalsa Coreco, Waterloo, Ontario, Canada. A total of 140 and 210 revolutions are acquired for two phantom measurements, covering 28 mm and 42 mm in the elevation direction. All simulations are based on the same geometry and movement. Post-processing is done using Matlab. Beamforming is performed with an up-sampled data-set to reduce interpolation errors.

Table I
Transducer and measurement parameters.

Transducer type	Single Element
Center frequency, f_0	6.0 MHz
Element radius	8.5 mm
Focus depth	25 mm
Rotation radius	5.3 mm
Emissions per revolution	900
Slice thickness	0.2 mm

IV. Results

To evaluate the ability of SAF to improve resolution in azimuth and elevation, a series of scatterers are simulated and measurements are performed on two phantoms. One phantom consists only of wires and is used to evaluate the improvements in resolution in the elevation direction. The second phantom has wires in both the lateral and elevation direction. Measurement and simulation positions on figures are indicated by the position of symbols. Measurement points are connected to visualize how the value between measurements is assumed to be. Beamforming is performed using a Hann apodization. This is done for 2D and 3D focusing and for simulations and measurements.

The resolution in both azimuth and elevation is first estimated independently through simulation. A set of scatterers are simulated between 15 and 100 mm of depth with a 5 mm spacing to represent both the near-field and far-field of the transducer. The evaluation will be done using the FWHM, MSLL, and gain in SNR to evaluate resolution, and penetration, respectively. FWHM is calculated from a maximum amplitude projection in the axial direction for each scatterer. The MSLL is defined as the mean value outside the main-lobe, where the main-lobe is defined as twice the width of the -20dB level. SNR is often estimated by several identical measurements. Because of the motion of the transducer, creating exact measurements will be very difficult. Instead, the gain in SNR is estimated using the result from SAF and for a fixed focused emission. The estimate is calculated by

$$\text{SNR}_{\text{gain}} = \frac{p_{\text{sp,saf}}^2}{p_{\text{sp,uf}}^2 \sum_{n=1}^{N} a_n^2}, \tag{6}$$

where $p_{\text{sp,saf}}$ is the amplitude at the spatial peak of the investigated scatterer, using a SAF beamforming approach, $p_{\text{sp,uf}}$ is the amplitude of the fixed focus approach, and a_n is the apodization value from (4).

A. Simulations

To evaluate the ability to focus in two dimensions simultaneously, the focusing in azimuth and elevation is evaluated for the single-plane SAF, as well as the two 3D SAF techniques. Fig. 2 shows the improvement in FWHM for single dimension SAF. It shows that SAF is able to hold a constant $F^{\#}$ in elevation for the desired depth, but is limited by the rotational axis in azimuth. Fig. 3 and 4 show that SAF focusing in both dimensions only has a slight effect on the resolution compared to single dimensional focusing.

Just as important as resolution in an ultrasound image is contrast, which is highly dependable on the amplitude of

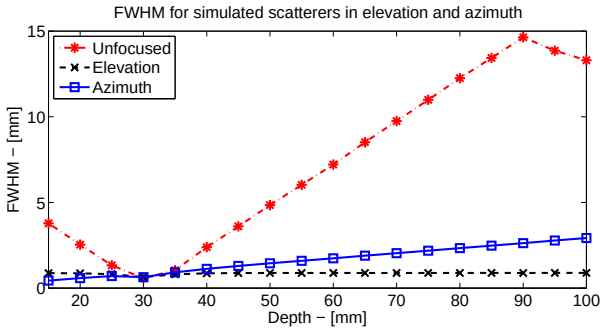

Figure 2. FWHM for simulated scatterers using single plane SAF in elevation and azimuth as well as fixed focus. The fixed focus is assumed to be identical in both azimuth and elevation.

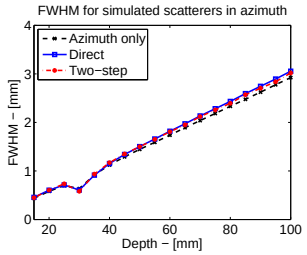

Figure 3. FWHM in azimuth for different focusing schemes. Single plane, direct, and two-step SAF.

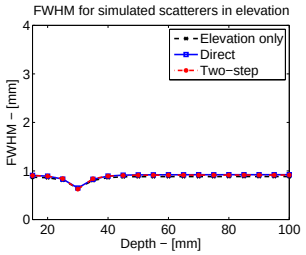

Figure 4. FWHM in elevation for different focusing schemes. Single plane, direct, and two-step SAF.

the side-lobes. Both methods have an MSLL in azimuth of ≈ -120 dB, which is far below the dynamic range currently used. For elevation the MSLL varies much more between the two methods. The direct 3D SAF method has elevation side-lobes below -60 dB but the two-step approach has very high side-lobes. By increasing the number of beamformed points for each line in the first beamforming step it is possible to reduce these side-lobes. Fig. 5 shows the MSLL for the direct and the two-step approach. The lines clearly show a reduction in side-lobes as the number of axial samples increases from 1,500 to 20,000 per line. The side-lobes are a result of errors in the interpolation step, which can be circumvented by either increasing the sampling density or by choosing a more advanced interpolation scheme [21]. To reduce the side-lobes below -60 dB a minimum of $\approx$ 10,000 samples per line are required. This amount has been used for all subsequent simulations and beamforming of phantom measurements.

From the simulation results it is seen that both the direct and two-step approach are able to give the same resolution and side-lobe level when applied to simulated scatterers, using an appropriate number of samples for the intermediate

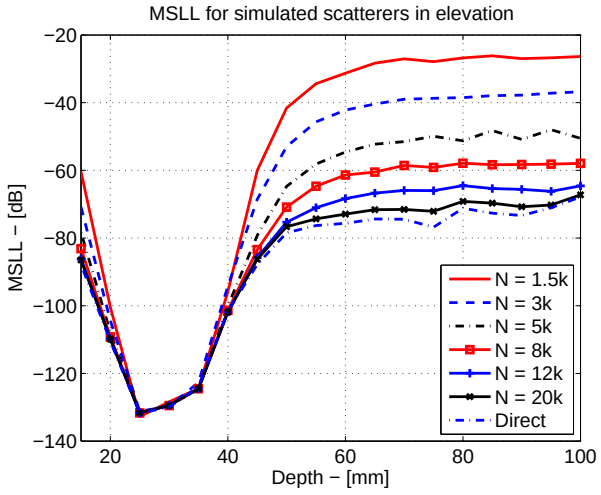

Figure 5. MSLL in elevation for different first step sampling distances and compared to direct 3D SAF. The depths of the simulation points are not indicated on all lines to avoid cluttering the graph, but is identical to the lines using 8000, 12000 and 20000 points.

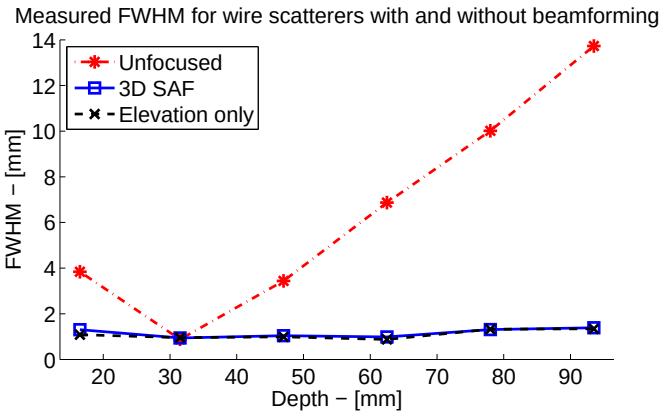

Figure 6. FWHM in the elevation direction of measured wire phantom. The FWHM is almost constant and unchanged regardless of whether only elevation focusing or full 3D focusing is used.

beamforming.

B. Phantom Measurement

To validate the simulation results a wire phantom in water and a complex speckle phantom designed specifically for this transducer has been measured. The wire phantom is used to validate the improvement in resolution in elevation for a simple setting. The more complex phantom allows the visualization of both scatterers in azimuth and elevation and speckle quality. Results from phantoms are only showed using the two-step method with adequate sampling density, as the results are almost identical with the direct method.

The wire phantom holds six wires placed between 15 and 90 mm of depth. The FWHM in the elevation direction before and after SAF is shown in Fig. 6. The values have a very high similarity with the simulated results. A difference is found in the mean FWHM, which for simulations is 0.89 mm, where the mean measured FWHM is 1.09 mm. Since the wire phantom is created with twisted wires, this might give rise to the increase in width. The figure also shows that

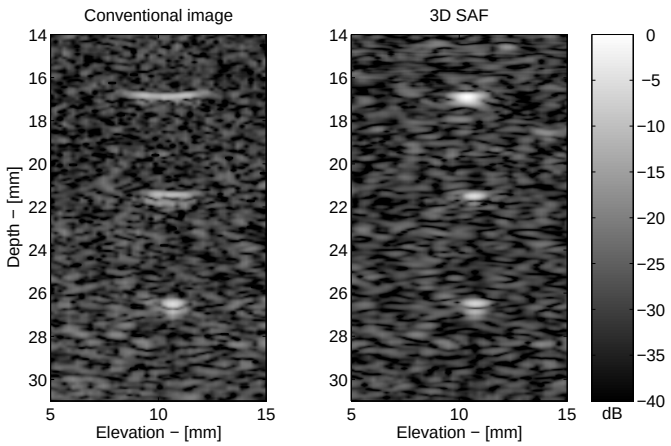

Figure 7. Comparison of three scatterers. The left image is created using conventional US imaging and the right is created by applying 3D SAF.

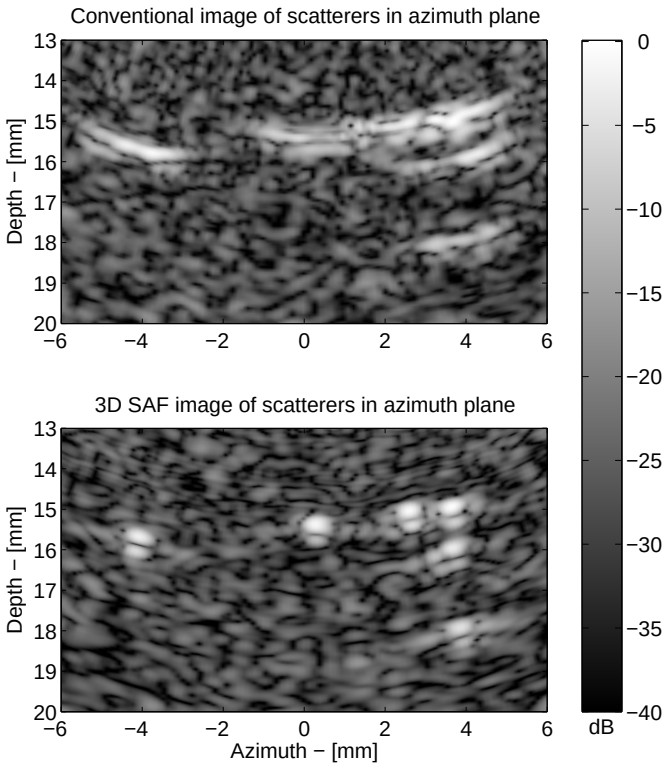

Figure 8. Several scatterers in azimuth with different distances and depths. The top image is created using conventional US imaging and the bottom is created by applying 3D SAF.

the improvement in resolution is the same for both 2D and 3D focusing, which is the same as what was found in simulations.

The results from the complex phantom are visualized using two different sections, which include scatterers created by wires in azimuth and elevation. Fig. 7 shows three wires in the elevation direction where the left image is the data as represented using the current system, and the right image is created using 3D SAF. Both scatterers and speckle are seen to be more uniform and depth independent when 3D SAF is applied.

Scatterers in azimuth are shown in Fig. 8. As for the elevation image the speckle is shown much more homogeneous and the scatterers are much more clearly resolved. The scatterers at the top are 10 mm from the transducer, which allows for a significant improvement in performance. The image created using 3D SAF resolves all the scatterers where the conventional image has trouble resolving the structure of three closely lying scatterers. The ability to resolve close scatterers will improve functionality in relation to tracking and positioning of seeds during prostate cancer treatment. It has yet to be seen whether the method is able to reduce shadowing below seeds.

C. Signal-to-Noise Ratio

Evaluating the change in SNR for the given movement using SAF is done by using simulations, wire phantom, and the speckle phantom. In all cases the amplitude is compared to that for the fixed focus scan-method as given in (6). Fig. 9 shows the estimated gain in SNR from simulations as well as the measured change in SNR from phantoms. The gain in SNR from the speckle phantom is estimated by the average amplitude of the speckle along a line only containing speckle instead of just the peak amplitude. The average is achieved by a moving average filter on the amplitude detected data. The estimated increase in SNR by simulations show an improvement in 20 to 30 dB outside the focal point. The drop in SNR at the focal point is caused by a discontinuity in the ToF calculations and for a real application will be changed to simply pass the original data for a limited region. Measurements do not give nearly as good an improvement in SNR as simulations estimate, with almost no improvement in the near-field and $\approx$15 dB below the transducer focus. The measurements for both the wire- and complex phantom agree well with each other and show that applying 3D SAF allows for an improved penetration; although not as good as simulations indicate. The reason for this reduced gain in SNR may come from simulations using only single scatterers and the measurements use speckle and wires, which might not behave as expected according to (6). Other sources of errors can be small differences in the behavior between the simulated and actual transducer, as well as effects caused by the outer transducer casing.

V. Processing

A single element transducer has very low processing requirements compared to linear arrays. This leaves system resources free to do more advanced processing. Real-time SA focusing in azimuth for a rotating array has been implemented in [3].

To implement a full 3D focusing increases the number of calculations significantly. It is possible to reduce the number of calculations by omitting some of the emissions by either creating a sparse sampling or increasing the $F^{\#}$. Sparse

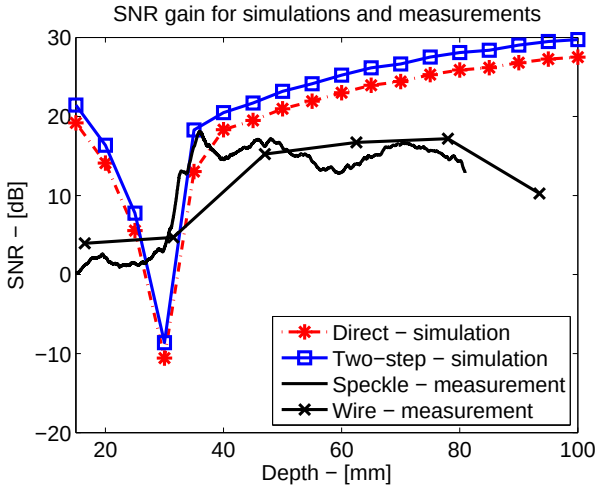

Figure 9. SNR increase by different SAF methods for simulated and measured scatterers.

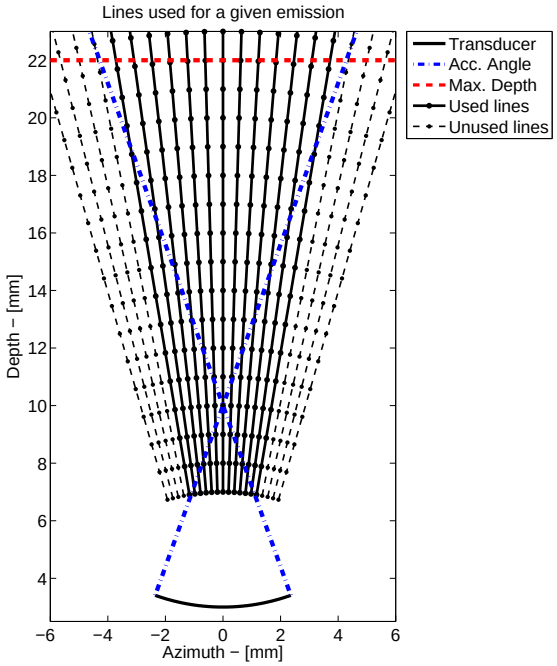

Figure 10. Visualization of the movement of a point relative to the transducer. The position of the virtual source is denoted r_{VS} and the rotation of the transducer is set at (0,0).

sampling can be applied intelligently to reduce the impact on side-lobes [22] or an increased $F^{\#}$ can be used at the expense of resolution. This section will only estimate the processing requirements for applying either two-step or direct 3D SAF, and not ways to reduce this. The results gained in Section IV-A will be used as a requirement for the number of points during the first step of the two-step approach.

Each emission is only able to contribute to a given number of lines, which are within the acceptance volume of the virtual source. The number of lines that will be beamformed per emission is set to that of the worst-case depth, regardless of whether most points along some of the lines are outside the acceptance angle. Exemplified: If 20 points are within the acceptance angle of an emission at the deepest point and 500 points are used per line, a total of 10,000 points are assumed to be beamformed. This is done even though many points closer to the transducer will have an apodization value of 0 due to the acceptance angle of the virtual source. This method is chosen to give a worst case estimate of what is required if implemented using FPGAs or multiple CPUs, which have to wait for new data or require synchronization. A visualization is shown in Fig. 10, which shows the discretization. The solid dotted lines are the beamformed lines for that emission, and the dashed lines are those omitted.

The required number of lines is largely dependant on the maximum desired increase in resolution and the largest distance from the elevation focus. The maximum number of lines used in elevation is given by

$$N_{\text{ele}}(z_{\max}) = \frac{|z_{\max} - z_{\text{VS}}|}{F^{\#}\Delta y} + 1, \tag{7}$$

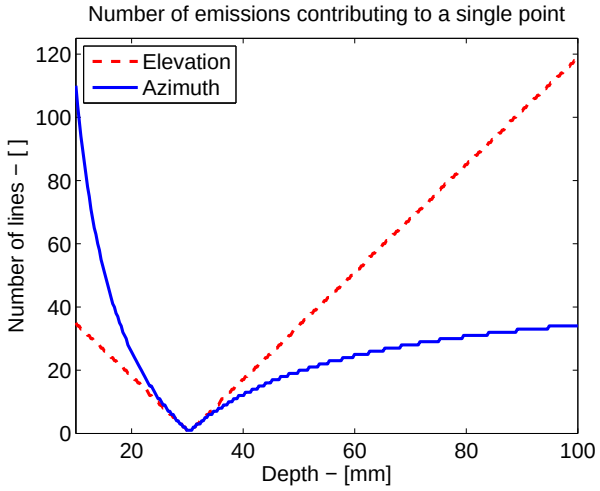

Figure 11. Number of lines required to be processed in elevation and azimuth for a given depth.

where $z_{\max}$ is the maximum depth required, z_{VS} is the depth of the virtual source used for beamforming, $F^{\#}$ is the f-number of the transducer, and Δy is the elevation distance between each emission for the same azimuth direction. The maximum number of emissions used in azimuth is given by the intersection of the point rotated on a circle and the elevation acceptance angle lines. The intersection is given by

$$\tilde{x} = \frac{\sqrt{z_{\max}^2\gamma - z_{\text{VS}}} - 2F^{\#}z_{\text{VS}}}{\gamma} \tag{8}$$

$$\tilde{z} = 2F^{\#}\tilde{x} + z_{\text{VS}} \tag{9}$$

where $\gamma = 1 + (2F^{\#})^2$. The total number of emissions for a given depth $z_{\max}$ is given by combining (8) and (9) into

$$N_{\text{azi}}(z_{\max}) = \frac{2}{\Delta\theta}\arctan\left(\frac{\tilde{x}}{\tilde{z}}\right) + 1, \tag{10}$$

where $\Delta\theta$ is the angular distance in azimuth between two emissions. Fig. 11 shows (7) and (10) as a function of depth. Since the aperture is rotating 5.3 mm from the center of the transducer the value of z_{VS} is increased. Otherwise all parameters are equal to those given in Table I. Here it is seen that the azimuth improvement is most costly close to the transducer surface and the elevation improvement becomes more expensive with increasing depth.

To calculate the number of lines for the direct SAF method, the number of lines for an emission will be described by an intersection between the conical acceptance volume of the tranducer and the cylinder motion. The expression is both very complex, and also has to be discrete. An approximation to the problem is used to give an indication of the progression of the number of calculations needed. The area of an ellipse is chosen with the number of lines from (7) and (10) used as the size of the major and minor axis, giving the total number of lines for each emission in a direct 3D SAF implementation equal to

$$N_{\text{direct}}(z_{\max}) = \pi N_{\text{ele}}(z_{\max})N_{\text{azi}}(z_{\max})M \tag{11}$$

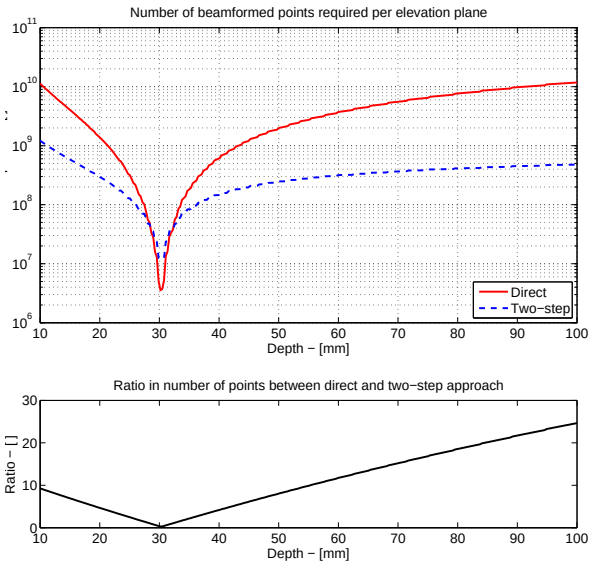

Figure 12. Number of points required to be processed per slice, assuming 900 lines per slice. The ratio between the two beamforming methods is shown at the bottom plot.

where M is the number of samples per line in the resulting volume. For each emission the two-step approach requires

$$N_{\text{two-step}}(z_{\max}) = N_{\text{azi}}(z_{\max})M_{\text{two-step}} + N_{\text{ele}}(z_{\max})M \quad (12)$$

where $M_{\text{two-step}}$ is the number of samples per beamformed line in the intermediate step of the two-step approach.

For an estimate of the total required number of beamformed points, the resulting volume is assumed to have 512 points per line and 900 lines per rotation. The two-step approach is set to have 12,000 samples per line to give side-lobes below -60 dB. The total required calculations for a given depth is shown in Fig. 12. This figure clearly shows that splitting beamforming in azimuth and elevation gives a reduction of around an order of magnitude. The two-step approach reduces the number of calculations, but requires an intermediate data-storage for the data after the azimuth focusing. This storage will equal the number of points beamformed, and the number of bytes is given by

$$B_{\text{storage}} = N_p N_l N_s B_d, \quad (13)$$

where N_p is the number of points per line, N_l is the number of lines, N_s is the number of elevation slices, and B_d is the bytes per point of data. For the setup used in this paper the total storage will be 9.1 GB of storage, assuming 16 bit complex data values and 210 slices of raw-data.

The two different approaches both have merits and drawbacks. The direct approach uses more processing than the two-step approach and has a constant processing requirement that will not change with either ultrasound resolution or scan-depth. The two-step approach allows big savings in calculations, but requires a large intermediate storage, and is largely invariant to the resulting image resolution since the expensive processing is defined by frequency, bandwidth, and scan-depth. The large storage can be alleviated by choosing a better interpolation step for the elevation beamforming step. Advanced interpolation will trade processing requirements for the first step, and storage space for a higher processing requirement on the second beamforming step.

VI. Conclusion

This paper shows that significant improvements can be obtained by using 3D SAF on a single element transducer. The spiral motion of the transducer allows both a direct 3D SAF method as well as a two-step approach to be implemented successfully. Both methods perform equally well with regards to improvements in resolution and side-lobe level.

For simulated scatterers an improvement in azimuth by up to a factor of 5 is possible, although resolution does decrease with depth. In elevation 3D SAF is able to maintain a constant FWHM equal to the found at the focal point of the transducer. A measurement of a wire phantom in elevation showed a slightly higher FWHM, but still independent of depth. Simultaneous improvements in azimuth and elevation resolution were shown in a complex phantom, consisting of wires in both azimuth and elevation significantly improving resolution. The improvement allowed for a clear separation of closely lying scatterers, which were otherwise overlapping. SNR was improved in measurements by $\approx$15 dB, at depths below the transducer focal point, allowing for either a better penetration, or the use of a higher center frequency, improving the image quality.

Computational costs of the two-step approach is of an order of magnitude lower compared to direct 3D SAF. The reduction in computations requires an intermediate storage of 9.1 GB. Choosing one method over the other is highly dependent on the system. If processing power is cheap compared to storage the direct method will be more efficient to implement and vice versa.

Acknowledgment

This work was supported by grant 71122 from the Danish Ministry of Science, Technology and Innovation, grant 9700883, 9700563 and 26-04-0024 from the Danish Science Foundation and by B-K Medical Aps, Denmark.

References

[1] A. Jemal, R. Siegel, E. Ward, Y. Hao, J. Xu, T. Murray, and M. J. Thun. Cancer statistics 2008. *CA Cancer Journal for Clinicians*, 58(2):71–96, 2008.

[2] R. G. Stock, N. N. Stone, M. F. Wesson, and J. K. DeWyngaert. A modified technique allowing interactive ultrasound-guided three-dimensional transperineal prostate implantation. *Int. J. of Radiation Oncology Biology Physics*, 32:219–225, 1995.

[3] J. Kortbek, J. A. Jensen, and K. L. Gammelmark. Synthetic aperture sequential beamforming. In *Proc. IEEE Ultrason. Symp.*, pages 966–969, 2008.

[4] L.J. Cutrona, E.N. Leith, L.J. Porcello, and W.E. Vivian. On the application of coherent optical processing techniques to synthetic-aperture radar. *IEEE Proc.*, 54:1026–1032, 1966.

[5] C. B. Burckhardt, P-A. Grandchamp, and H. Hoffmann. An experimental 2 MHz synthetic aperture sonar system intended for medical use. *IEEE Trans. Son. Ultrason.*, 21(1):1–6, January 1974.

[6] G. S. Kino, D. Corl, S. Bennett, and K. Peterson. Real time synthetic aperture imaging system. In *Proc. IEEE Ultrason. Symp.*, pages 722–731, 1980.

[7] K. Nagai. A new synthetic-aperture focusing method for ultrasonic *B*-scan imaging by the fourier transform. *IEEE Trans. Son. Ultrason.*, SU-32(4):531–536, 1985.

[8] J. T. Ylitalo and H. Ermert. Ultrasound synthetic aperture imaging: monostatic approach. *IEEE Trans. Ultrason., Ferroelec., Freq. Contr.*, 41:333–339, 1994.

[9] C. H. Frazier and W. D. O'Brien. Synthetic aperture techniques with a virtual source element. *IEEE Trans. Ultrason., Ferroelec., Freq. Contr.*, 45:196–207, 1998.

[10] J. Kortbek, J. A. Jensen, and K. L. Gammelmark. Synthetic Aperture Focusing Applied to Imaging Using a Rotating Single Element Transducer. In *Proc. IEEE Ultrason. Symp.*, pages 1504–1507, Oct. 2007.

[11] J. A. Jensen and N. B. Svendsen. Calculation of pressure fields from arbitrarily shaped, apodized, and excited ultrasound transducers. *IEEE Trans. Ultrason., Ferroelec., Freq. Contr.*, 39:262–267, 1992.

[12] J. A. Jensen. Field: A program for simulating ultrasound systems. *Med. Biol. Eng. Comp.*, 10th Nordic-Baltic Conference on Biomedical Imaging, Vol. 4, Supplement 1, Part 1:351–353, 1996b.

[13] C. Passmann and H. Ermert. A 100-MHz ultrasound imaging system for dermatologic and ophthalmologic diagnostics. *IEEE Trans. Ultrason., Ferroelec., Freq. Contr.*, 43:545–552, 1996.

[14] M. Karaman, P. C. Li, and M. O'Donnell. Synthetic aperture imaging for small scale systems. *IEEE Trans. Ultrason., Ferroelec., Freq. Contr.*, 42:429–442, 1995.

[15] M. H. Bae and M. K. Jeong. A study of synthetic-aperture imaging with virtual source elements in B-mode ultrasound imaging systems. In *IEEE Trans. Ultrason., Ferroelec., Freq. Contr.*, volume 47, pages 1510–1519, 2000.

[16] S. I. Nikolov and J. A. Jensen. Virtual ultrasound sources in high-resolution ultrasound imaging. In *Proc. SPIE - Progress in biomedical optics and imaging*, volume 3, pages 395–405, 2002.

[17] H. Andresen, S. I. Nikolov, M. M. Pedersen, D. Buckton, and J. A. Jensen. Three-dimensional synthetic aperture focusing using a rocking convex array transducer. *IEEE Trans. Ultrason., Ferroelec., Freq. Contr.*, 57:1051–1063, 2010.

[18] S. I. Nikolov and J. A. Jensen. 3D synthetic aperture imaging using a virtual source element in the elevation plane. In *Proc. IEEE Ultrason. Symp.*, volume 2, pages 1743–1747, 2000.

[19] K. Gammelmark. *Improving the Image Quality of Synthetic Transmit Aperture Ultrasound Images*. PhD thesis, Ørsted•DTU, Technical University of Denmark, 2800, Lyngby, Denmark, 2004.

[20] S. I. Nikolov, J. A. Jensen, and B. G. Tomov. Fast parametric beamformer for synthetic aperture imaging. *IEEE Trans. Ultrason., Ferroelec., Freq. Contr.*, 55:1755–1767, 2008.

[21] J. Kortbek, H. Andresen, S. Nikolov, and J. A. Jensen. Comparing interpolation schemes in dynamic receive ultrasound beamforming. In *Proc. IEEE Ultrason. Symp.*, pages 1972–1975, 2005.

[22] G. R. Lockwood, J. R. Talman, and S. S. Brunke. Real-time 3-D ultrasound imaging using sparse synthetic aperture beamforming. *IEEE Trans. Ultrason., Ferroelec., Freq. Contr.*, 45:980–988, 1998.